ELSEVIER

Journal of Alloys and Compounds 389 (2005) 102–112

Journal of ALLOYS AND COMPOUNDS

www.elsevier.com/locate/jallcom

Terminal solid solubility of hydrogen in Zr-alloy pressure tube materials

R.N. Singh[a,*], S. Mukherjee[a], Anuja Gupta[b], S. Banerjee[a]

[a] *Materials Science Division, Bhabha Atomic Research Centre, Trombay, Mumbai 400 085, India*
[b] *Department of Metallurgy and Materials Engineering, IIT Roorkee, Uttaranchal 247 667, India*

Received 26 May 2004; received in revised form 29 July 2004; accepted 29 July 2004

Abstract

In this work, terminal solid solubility (TSS) of hydrogen for Zr-alloy pressure tube materials was determined corresponding to end of hydride dissolution (TSSD) and start of hydride precipitation (TSSP) using the dilatometry technique. For this, Zircaloy-2 and Zr–2.5Nb pressure tube alloy coupons were gaseously charged with controlled amount of hydrogen in the range 10–100 μg/g. Change in length of cylindrical specimens of length ∼10 mm and diameter ∼3.5 mm machined from the coupons were measured as a function of temperature using a dilatometer. The samples were heated at 2 °C/min to 430 °C, held for 30 min at 430 °C and cooled back to the ambient temperature at 2 °C/min. The transition temperatures corresponding to the end of dissolution of hydrides during heating and beginning of precipitation of hydrides during cooling in these alloys were determined from thermal strain (e) versus temperature (T), average slope (of e versus T plot) versus T and differential thermal strain versus T plots. The enthalpies of hydride dissolution and precipitation for Zircaloy-2 pressure tube material were found to be 30–34.5 and 25.9–26.3 kJ/mol, respectively, whereas the corresponding enthalpies for Zr–2.5Nb pressure tube material were found to be 35.44 and 17.2–22.8 kJ/mol, respectively. This difference in the enthalpies between TSSD and TSSP is explained in terms of the different roles played by the components of strain energy associated with the elastic and plastic deformation in the matrix and precipitate, as a result of hydride accommodation in this alloy during heating and cooling process.
© 2004 Elsevier B.V. All rights reserved.

Keywords: Precipitation; High temperature alloys; Thermal analysis; Zircaloy-2; Zr–2.5Nb alloy; Dilatometry

1. Introduction

Dilute zirconium alloys are used as the core structural materials of pressurized heavy water reactors (PHWR) because of their low neutron absorption cross-section, good elevated temperature mechanical properties and adequate aqueous corrosion resistance [1–7]. Though the hydrogen content of the in-core components is kept as low as possible by controlling the manufacturing process parameters [8], it can pick up hydrogen/deuterium during service from corrosion reaction between zirconium metal and coolant heavy water [7–12]. Hydrogen present in excess of solid solubility precipitates out as brittle hydride phase [13–21] and can severely limit the life of core components [22–24] made up of these alloys. The hydrogen-related problems associated with these components are hydride embrittlement [22–24] which gets aggravated due to stress-reorientation of hydride [25–31], delayed hydride cracking (DHC) [30–36] and hydride blister formation [30,37–41]. Initially, TSS was thought to be a safe limit for hydrogen concentration, below which embrittlement effect was not considered significant. However, recent studies have shown that the threshold hydrogen concentration for DHC initiation [32,36] and hydride blister nucleation [41,42] are not TSS but a fraction of TSS. Thus, terminal solid solubility of hydrogen in these alloys is an important parameter and is used by design and safety engineers for fitness for service assessment of these components [43].

Experimentally TSS is determined by preparing samples with known concentration of hydrogen and measuring some change in physical properties to identify transition temperature corresponding to end of hydride dissolution during heating and beginning of hydride precipitation during cooling. Techniques like dilatometry [44,45], resistivity [46], internal

* Corresponding author. Tel.: +91 22 25593814; fax: +91 22 25505151.
E-mail address: mms@apsara.barc.ernet.in (R.N. Singh).

0925-8388/$ – see front matter © 2004 Elsevier B.V. All rights reserved.
doi:10.1016/j.jallcom.2004.07.048

friction [47–49], differential scanning calorimetry [50–53], small angle neutron scattering [54,55], metallography [56] and thermal diffusion [57] measure changes in dimension, resistance, damping frequency, heat flow, lattice parameter, microstructural features and H concentration, respectively, and are used to determine the transition temperature. The experimentally determined transition temperatures are correlated with corresponding hydrogen concentrations in the form of an Arrhenius type relationship to obtain the pre-exponential constant and the enthalpy of the dissolution or precipitation process. With the help of these constants, TSS at any temperature can be obtained. Also, for a sample of unknown hydrogen concentration by determining the transition temperature corresponding to heating and/or cooling total hydrogen content of the sample can be estimated using the aforementioned constants.

Two series of dilute Zr alloys are being extensively used as pressure tube material in PHWR type reactors. Early generation PHWRs use tubes made of Zircaloy-2, an alloy with tin as primary alloying addition. Although pressure tubes of this material served satisfactorily in reactor applications, it is now known that Zircaloy-2 suffers from high rates of hydrogen pick up and somewhat high rates of irradiation induced creep [58]. The next important alloy is Zr–2.5 wt.% Nb (Zr–2.5Nb) [5–8,58] that has been chosen as a pressure tube material for new generation PHWRs. The Zr–2.5Nb alloy has been tried in two different conditions: conventional cold work and stress relieved and heat treated (quenched and tempered) state [59]. The microstructure of cold worked and stress relieved (CWSR) Zircaloy-2 consists of elongated and textured α Zr-phase (having hcp crystal structure) grains with a small amount of randomly distributed fine intermetallic precipitates [1–5]. On the other hand the microstructure of CWSR Zr–2.5Nb alloy is comprised of heavily elongated and strongly textured α phase grains surrounded by very thin but nearly continuous grain-boundary network of metastable β phase (having bcc crystal structure with 10–20% Nb and volume fraction in the range of 10–20%) [1–6,53,60]. McMinn et al., based on their investigations of a series of Zircaloys [61], have observed negligible influence of chemical composition and microstructure on TSS. Khatamian [52,53] investigated the TSS and partitioning of hydrogen in a series of Zr–Nb alloys in metastable (containing β-Zr with 20% Nb) and aged (containing β Nb with greater than 85% Nb) condition and has reported increase in hydrogen solubility for metastable alloy with increasing Nb content (or increasing β phase volume fraction). However, for the completely aged Zr–Nb alloys, TSS values were comparable to that for Zircaloys [52].

Thus, it is felt that the TSS of hydrogen in Zr–2.5Nb alloy pressure tube material containing metastable β-Zr phase must be higher compared to that for Zircaloys. The objective of this study is to determine the TSS of hydrogen in CWSR Zircaloy-2 and Zr–2.5Nb pressure tube materials used in the Indian PHWRs. Hydride precipitation in Zr-alloys is associated with a large positive volume change. One of the consequences of this large volume change is the local deformation of the matrix to accommodate the hydride precipitates. Based on the strain energy associated with elastic and plastic deformation of the matrix, Puls [33,59] developed a theoretical model of TSS of hydrogen in Zr-alloys. Experimentally observed values of TSS show large hysteresis between the values obtained during heating and cooling. TSS obtained during heating corresponds to the end of hydride dissolution and is called TSSD whereas TSS obtained during cooling corresponds to the beginning of hydride precipitation and is called TSSP. In this work both TSSD and TSSP values determined using dilatometry technique are discussed for Zr-alloy pressure tube materials.

2. Experimental

The Zircaloy-2 and Zr–2.5Nb pressure tube material was received from Nuclear Fuel Complex, Hyderabad, in autoclaved (cold worked and stress-relieved) condition. Typical chemical compositions of Zircaloy-2 and Zr–2.5Nb tubes are given in Table 1 [63]. Coupons of length 50 mm, width 20 mm were cut from the tube and were polished up to 1200 grit emery paper to obtain oxide free surface. The polished samples were gaseously charged with controlled amount of hydrogen in a modified Sieverts' apparatus [51,64]. In the present set of investigations, the samples were furnace cooled after hydrogen charging at 363 °C with an average cooling rate of ∼2 °C/min. To reveal the hydride morphology, orientation and distribution, the gaseously charged samples were sectioned along the radial-circumferential and axial-radial plane of the tube and metallographically examined under optical microscope. Before examination under optical microscope, the Zircaloy-2 samples were chemically etched by swabbing for 30 s with cotton soaked in 8% HF in HNO_3 solution [24] while the Zr–2.5Nb samples were etched by swabbing for 20 s with cotton soaked in 10%HF + 45%HNO_3 + 45%H_2O solution.

Table 1
Typical chemical composition of Zircaloy-2 and Zr–2.5Nb alloy pressure tube material depicting the weights of constituent alloying elements in percent [63]

Elements	Zircaloy-2	Zr–2.5%Nb
Tin	1.20–1.70	–
Iron	0.07–0.20	–
Chromium	0.05–0.15	–
Nickel	0.03–0.08	–
Niobium	–	2.40–2.80
Total Fe + Cr + Ni	0.18–0.38	–
Total Fe + Cr	–	–
Carbon (ppm)	150–400	–
Oxygen (ppm)	900–1400	900–1300
Copper	–	–
Zr + permitted impurities	Balance	Balance

2.1. Dilatometry

Solid cylindrical samples of length ~10 mm and diameter ~3.5 mm were machined from the hydrided Zr-alloy coupons. These cylindrical samples were subjected to a thermal cycle during which change in length of the sample was measured using a Dilatometer model DIL 805 A/D. The samples were inductively heated. The heating rate was controlled by controlling the induced current passing through the specimen and the cooling rate was controlled by controlling the gas flow in addition to induced current. The temperature was measured using Rh/Pt thermocouple spot welded to the sample. The test data comprising of temperature, time and change in length was acquired digitally through automated software. The change in length was measured using a LVDT of resolution 50 nm. The resolution of temperature measurement was 0.05 °C. In the present investigation, the temperature program involved heating the samples at a rate of 2 °C/min to 430 °C, soaking for a period of 30 min at 430 °C and then cooling back to the room temperature at the 2 °C/min. The soaking temperature and time was chosen so as to dissolve all the hydrides, anneal out the dislocation debris left out in the matrix after hydride dissolution. In fact this dislocation debris is reported to impart memory effect to hydride precipitation during cooling and influences the TSSP temperature [31,47].

2.2. TSS determination

Raw data comprising of change in length of the sample (ΔL) and its temperature was obtained from dilatometer using automated software. A thermal strain (e) versus sample temperature (T) plot was obtained from the raw data. The transition temperatures corresponding to end of hydride dissolution during heating and beginning of hydride precipitation during cooling were obtained for Zr-alloy samples, which have been hydrided to different hydrogen concentrations. TSS is determined by fitting an Arrhenius type relationship given in Eq. (1) between the hydrogen concentration and transition temperature. For this the log of hydrogen concentration was plotted against the inverse of absolute transition temperature and the pre-exponential constant, A, and the enthalpy of the process, ΔH, were obtained by linear regression analysis. Since temperature is a part of the argument of the exponential term, the TSS value is very sensitive to temperature. Any error in determination of the transition temperature will translate into the error in the estimated hydrogen content of the unknown sample. Hence, it is necessary to determine the transition temperature accurately:

$$\mathrm{TSS} = A \exp\left(-\frac{\Delta H_s}{RT}\right) \quad (1)$$

It was observed that for smaller hydrogen concentration the transition temperature corresponding to hydride dissolution and precipitation were not clearly identifiable from the e versus T plot. This problem was overcome by defining average slope (m) and plotting its variation with temperature. The average slope, m, is defined in

$$m = \frac{\Delta L_i - \Delta L_r}{T_i - T_r} \quad (2)$$

where, ΔL is the change in length, T the temperature and the subscript i and r refer to instantaneous and reference values. The plot of m against temperature shows a clear transition and facilitates more precise determination of the transition temperature. Another method employed in the present investigation for obtaining the transition temperature was to plot the differential strain with temperature. For this, unhydrided Zircaloy-2 sample containing <10 μg/g of hydrogen and Zr–2.5Nb sample containing 5.6 μg/g of hydrogen were used. The differential strain was taken as the difference between the strains of the hydrogen charged sample and that of the unhydrided one. Thus, the transition temperatures corresponding to end of dissolution and beginning of precipitation of hydrides in Zr-alloys during heating and cooling, respectively, were obtained from all the three methods mentioned above.

The samples used for dilatometry measurement were sectioned using a slow speed cutoff wheel to obtain a piece of weight ~100–130 mg. The cut samples were ultrasonically cleaned in carbon tetrachloride bath. All the surfaces of the sectioned specimen were polished to remove the surface layer and were chemically analyzed for hydrogen concentration by using inert gas fusion (IGF) technique using LECO Hydrogen Determinator, Model RH IE. Titanium pellets containing 37.2 ± 4.1 μg/g hydrogen was used as reference material. The measurement uncertainty was found to be ~3.3 μg/g. Hydrogen concentrations charged into the coupons (as estimated by Sieverts' apparatus) [64] is compared with that determined by IGF in Table 2. Hydrogen concentration obtained by IGF was plotted against inverse of absolute transition temperature on semi-log plot to obtain the value of pre-exponential constant and the enthalpy of the process and only those values of these constants were accepted for which regression coefficient was greater than 90%.

3. Results

3.1. Hydride microstructure

Fig. 1 shows the micrograph of Zircaloy-2 pressure tube material charged with (a) 43 μg/g and (b) 107 μg/g of hydrogen. The micrograph corresponds to radial-circumferential section of the tube. Dark lines in these micrographs are the traces of hydrides. It is evident from these micrographs that with increasing hydrogen content level, the length of hydride platelets increases, though no significant decrease in the interplatelet spacing is observed. Fig. 2 shows the micrograph of the Zr–2.5Nb pressure tube material charged (a) 39 μg/g and (b) 80 μg/g of hydrogen concentrations. The hydrogen content values for both Zircaloy-2 and Zr–2.5Nb alloy reported above were estimated by IGF technique. The micro-

Table 2
The transition temperature (°C) corresponding to dissolution (*D*) and precipitation (*P*) of hydrides in Zircaloy-2 and Zr–2.5Nb alloy pressure tube material obtained from all the three curves

Material	*H* (ppm)	(*e* vs. *T*) *D*(*P*)	(*m* vs. *T*) *D*(*P*)	(Diff. *e* vs. *T*) *D*(*P*)
Zircaloy-2	43	255 (213)	262 (213)	265 (213)
	65	308.2 (232)	307.5 (231)	310.6 (233)
	86	−(265)	−(263)	−(262)
	92	324.4 (260)	324.4 (266)	324.4 (267)
	100	331.4 (277)	331.4 (275)	337.2 (276)
Zr–2.5Nb alloy	27.4	–	−(167.6)	277 (229)
	42.9	307 (207)	−(205)	–
	56.4	−(230)	−(235)	313 (236)
	58.3	344 (253)	347 (268)	344 (264)
	90	371 (301)	361 (289)	362 (286)

The hydrogen contents were measured by inert gas fusion technique.

graph corresponding to both radial-circumferential (RC) and axial-radial (AR) plane of the tube are shown in Fig. 2. The trace of hydride along the axial direction of the tube was longer as compared to the trace along circumferential direction. It can be inferred from these micrographs that for the both the materials, the hydride platelets were oriented predominantly along circumferential-axial plane of the tube.

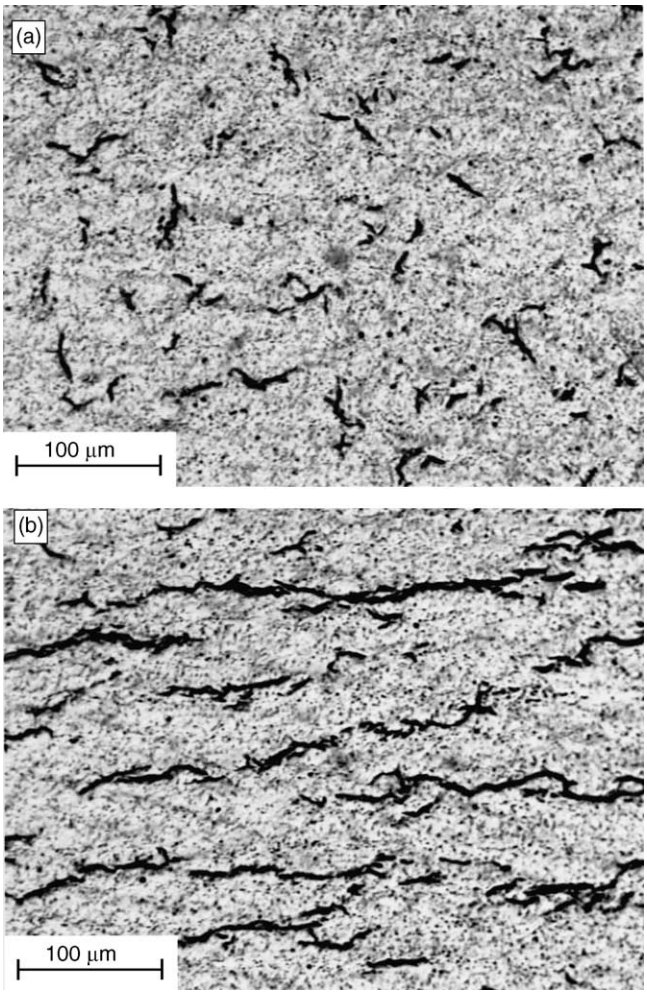

Fig. 1. Micrographs of Zircaloy-2 pressure tube material along the radial-circumferential (RC) section of the tube. The coupons were gaseously charged with (a) 43 μg/g and (b) 107 μg/g of hydrogen. As can be seen, the length of the hydride increases with the increase in hydrogen concentration.

3.2. Hydrogen content estimation

The average hydrogen (H) content of the H-charged Zircaloy-2 and Zr–2.5Nb coupons were estimated by Sieverts' method [64]. Hydrogen content was also determined by IGF technique by cutting small pieces from both Zircaloy-2 and Zr–2.5Nb alloy samples which were used for dilatometric measurement. The length of the hydrogen analysis samples was about half the length of the dilatometry sample. The hydrogen content of these samples is shown in Table 2 for both Zircaloy-2 and Zr–2.5Nb pressure tube alloys. These hydrogen concentration values obtained by IGF were used in the linear regression analysis with the transition temperatures corresponding to heating and cooling to obtain the Arrhenius parameters (A and ΔH_s) defined in Eq. (1).

3.3. Transition temperature determination

Thermal strain (e) is defined as the ratio of change in length with respect to a reference length. The transition temperatures corresponding to end of dissolution of hydrides during heating and beginning of precipitation of hydrides during cooling were obtained from thermal strain versus temperature (T) plots. A typical plot for Zr–2.5Nb pressure tube alloy containing 58.3 and 90 μg/g of hydrogen obtained during heating is shown in Fig. 3. The corresponding transition temperatures during heating were 344 and 371 °C, respectively. And the corresponding transition temperatures for these samples obtained during cooling were 253 and 301 °C, respectively (Table 2).

It was observed that the transition temperatures obtained from e versus T plots were not very distinct, especially at lower hydrogen concentration. One of the consequences of this is the inability to determine the transition temperature precisely. Thus, the average slope of the e versus T plot (m as defined in Eq. (2)) was computed and its variation with temperature was plotted. Typical m versus T plots obtained

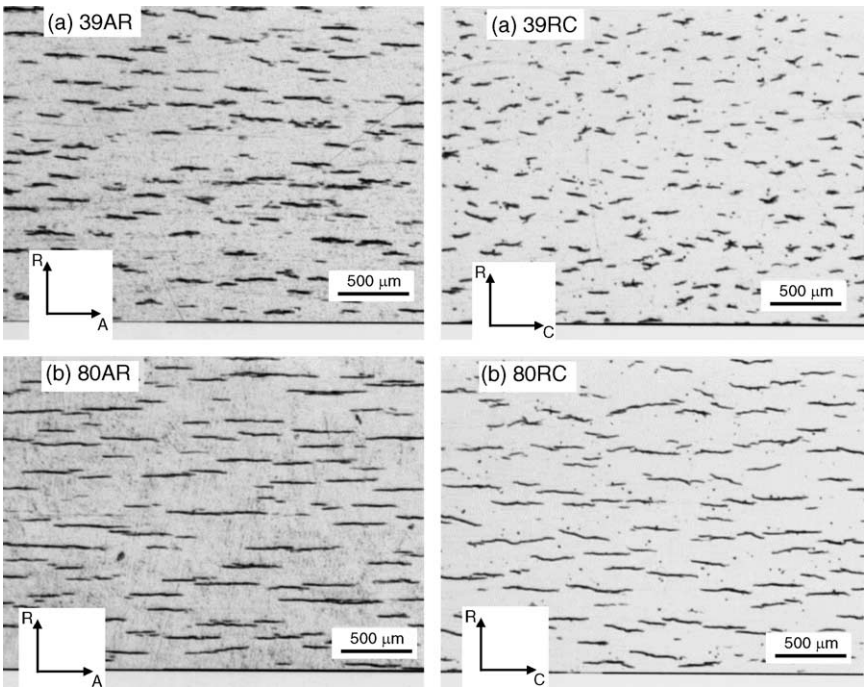

Fig. 2. The microstructural features of traces of hydrides on two orthogonal planes (AR: axial-radial; RC: radial-circumferential) of Zr–2.5Nb pressure tube alloy charged with (a) 39 μg/g and (b) 80 μg/g of hydrogen. The hydrogen concentration values were estimated by IGF technique.

during cooling for the Zircaloy-2 samples is shown in Fig. 4. Differential strain was determined by calculating the difference between thermal strain of the hydrided specimen and the unhydrided specimen. The variation in differential strain with temperature during heating for Zircaloy-2 samples containing different amount of hydrogen is shown in Fig. 5.

The transition temperatures obtained from *e* versus *T* plots, *m* versus *T* plots and differential strain (Diff. *e*) versus *T* plots for both the materials are listed in Table 2. The transition temperature was observed to increase with increasing hydrogen content and for given hydrogen concentration the transition temperature obtained during heating was higher than that obtained during cooling.

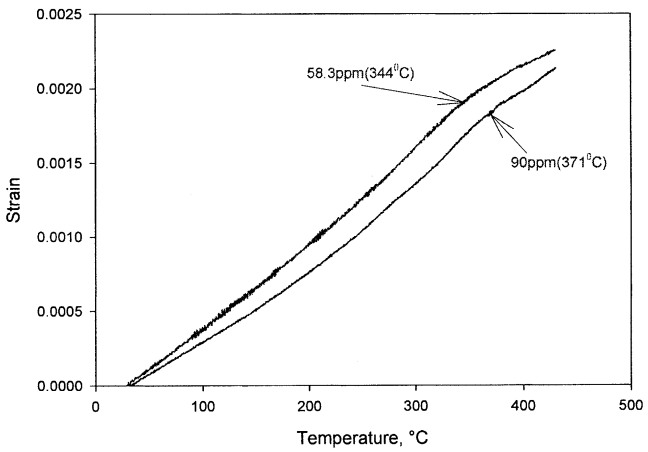

Fig. 3. A typical strain (*e*) vs. temperature (*T*) plot for the Zr–2.5Nb samples containing 58.3 and 90 μg/g of hydrogen obtained during heating.

3.4. Determination of Arrhenius parameters

The transition temperatures corresponding to end of dissolution and beginning of precipitation of hydrides in Zircaloy-2 and Zr–2.5Nb pressure tube material determined in the present investigation using all the three techniques described in Section 3.3 are summarized in Table 2. The hydrogen contents of the samples obtained from these samples which were used for dilatometry were estimated using IGF technique and are also given in this table. The values of pre-exponential constant and enthalpy of the process determined during heat up and cool down cycle are given in Table 3 for both Zircaloy-2

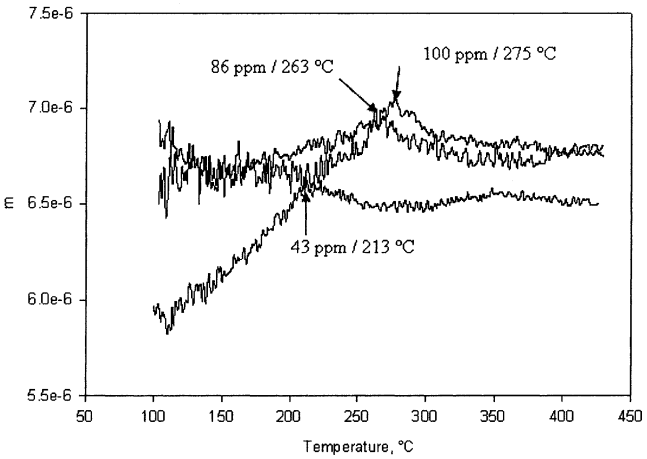

Fig. 4. The variation in average slope (*m*) with temperature obtained during cooling for Zircaloy-2 pressure tube samples charged with different hydrogen concentrations.

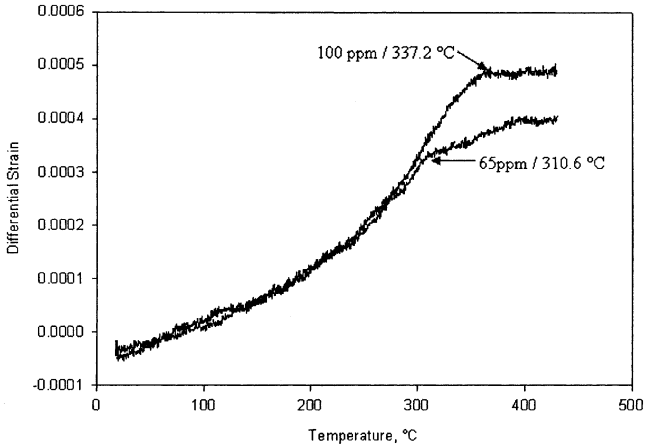

Fig. 5. The variation in differential strain with temperature obtained during heating for Zircaloy-2 pressure tube samples charged with different hydrogen concentrations.

and Zr–2.5Nb (in parenthesis) pressure tube materials. The pre-exponential constant and the enthalpy values are shown only for those data sets for which regression coefficient was greater than 90%. It can be seen from Table 3 that for the pressure tube material the enthalpy of dissolution of hydrides was higher compared to the enthalpy of precipitation of hydrides in these alloys.

4. Discussion

The maximum amount of hydrogen which can be retained in solid solution without forming hydride precipitate is called terminal solid solubility (TSS). TSS of hydrogen in zirconium alloys is observed to increase with increase in temperature. At ambient temperature TSS of hydrogen in zirconium alloys is less than 1 μg/g [44–57]. Hence, at ambient temperature almost all the hydrogen in zirconium alloy will be present as hydride. When a Zr-alloy sample containing hydride is heated, with increase in temperature, TSS increases resulting in dissolution of hydride in the matrix. For zirconium alloys hydride dissolution is associated with increase in sample volume. On the other hand, when zirconium alloy sample containing hydrogen is cooled down, hydride precipitation takes place resulting in decrease in sample volume. Using dilatometer, it is possible to detect the temperature corresponding to end of hydride dissolution during heating and beginning of hydride precipitation during cooling. For a given hydrogen concentration, the temperature corresponding to end of dissolution is called T_{TSSD} and the temperature corresponding to beginning of precipitation is called T_{TSSP}. On the other hand for a given temperature the amount of hydrogen in solution during heating and cooling are called TSSD and TSSP, respectively.

In the present investigation, both T_{TSSD} and T_{TSSP} for hydrogen in Zircaloy-2 and Zr–2.5Nb pressure tube material was determined using dilatometry from *e* versus *T* plots, *m* versus *T* plots and differential strain (Diff. *e*) versus *T* plots. The value of the Arrhenius parameters for Zircaloy-2 and Zr–2.5Nb pressure tube material are listed in Table 3.

The values of TSSD and TSSP obtained by the three methods were in good agreement. Though very small scatter was observed between the TSSD values obtained in the present investigation, the TSSP values obtained from the three methods (Section 3.3) were nearly identical. It may be noted that for Zr–2.5Nb pressure tube material regression analysis of TSSD temperature obtained using average slope and differential strain method with H-content yielded poor correlation coefficient and hence were discarded. The TSSP values for Zr–2.5Nb pressure tube alloy could be obtained from all the three (Section 3.3) methods, though a large scatter was observed between the TSSP values for Zr–2.5Nb pressure tube alloy as compared to that obtained for Zircaloy-2 in the present investigation.

4.1. TSSD

The variation in TSSD values for Zircaloy-2 and Zr–2.5Nb pressure tube material obtained in the present investigation are compared in Fig. 6. As can be seen from this figure, for constant hydrogen concentration the end of hydride dissolution temperature (T_{TSSD}) for Zr–2.5Nb pressure tube material is higher than that for Zircaloy-2 pressure tube material. It has been reported that β Zr phase has higher affinity and solubility of hydrogen [61]. Similarly, crystal defects like grain boundaries and dislocations can pin the interstitial hydrogen atoms. Thus presence of β Zr phase and crystal defect

Table 3
The pre-exponential constant *A* and enthalpy of the hydride dissolution or precipitation obtained during heating and cooling for Zircaloy-2 and Zr–2.5Nb alloy (in parentheses) pressure tube materials

Transition temperature obtained from (°C)	ΔH_s (kJ/mol)	*A*	Regression coefficient
Heat up cycle			
Strain vs. temperature	30.003 (35.44)	38177.7 (63576.55)	0.9352 (0.95)
m vs. temperature	33.78	81626.0	0.9554
Differential strain vs. temperature	34.55	94041.5	0.9192
Cool down cycle			
Strain vs. temperature	25.93 (17.21)	28536.5 (3235.6)	0.9626 (0.96)
m vs. temperature	26.00 (17.99)	29250.0 (3789.5)	0.9573 (0.94)
Differential strain vs. temperature	26.315 (22.82)	31236.0 (12209.8)	0.9663 (0.99)

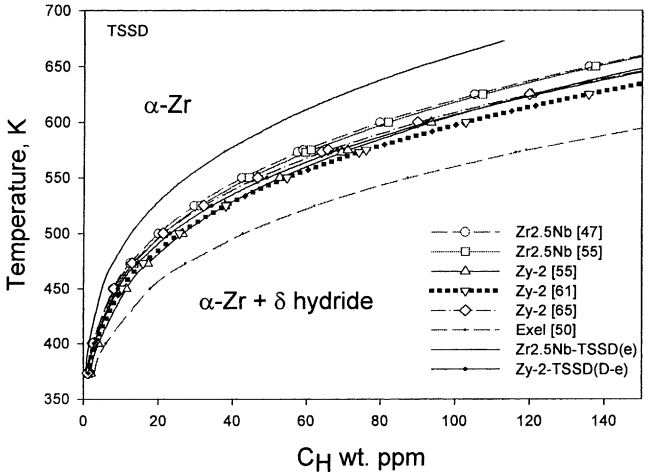

Fig. 6. Comparison of variation in TSSD for Zircaloy-2 and Zr–2.5Nb pressure tube alloy obtained in the present investigation with the TSSD values for these alloys reported in literature (shown in the bracket).

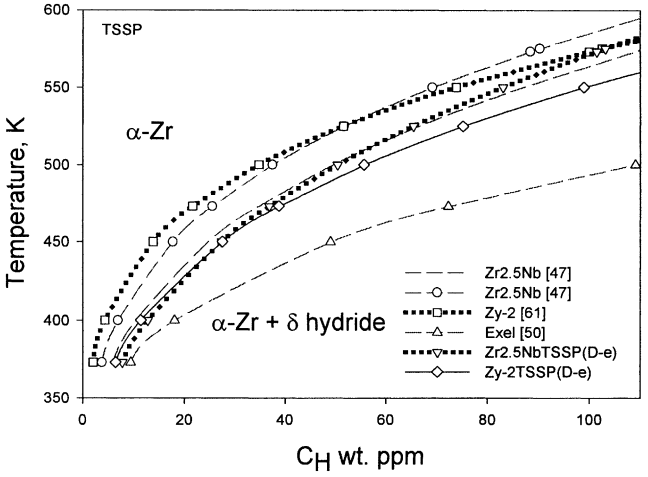

Fig. 7. Comparison of variation in TSSP for Zircaloy-2 and Zr–2.5Nb pressure tube alloy obtained in the present investigation with the TSSP values for these alloys reported in literature (shown in the bracket).

like grain-boundaries and dislocations delay the end of dissolution process [47,61] and thereby yielding higher value of T_{TSSD} for Zr–2.5Nb pressure tube alloy during heating as compared to that for Zircaloy-2.

In Fig. 6 the TSSD values obtained in the present investigation is also compared with the TSSD values reported in literature [45,47,50,61,62,65] for these alloys. It may be noted that for constant H-concentration the T_{TSSD} values for Zr–2.5Nb pressure tube material reported by Pan et al. [47] and Slattery [45] is higher than the T_{TSSD} values reported for Zircaloy-2 by Slattery [45], McMinn et al. [57] and Kearns [65]. However, the difference in the T_{TSSD} values of both the alloys reported in literature [45,47,50,61,65] is not significant. For a given hydrogen concentration, the T_{TSSD} values obtained in the present investigation for Zr–2.5Nb pressure tube alloy was much higher than those reported in literature. The TSSD values for Excel alloy [50] has also been compared in this figure. For a given temperature, the maximum amount of dissolved hydrogen in Zr–2.5Nb pressure tube alloy was least, while that in Excel was largest.

4.2. TSSP

The variation in TSSP values obtained in the present investigation for Zircaloy-2 and Zr–2.5Nb pressure tube material is compared in Fig. 7. Below a hydrogen concentration of 40 μg/g, the temperature corresponding to start of hydride precipitation (T_{TSSP}) for Zr–2.5Nb pressure tube material was observed to be lower than that for Zircaloy-2. For hydrogen concentration in between 40 and 70 μg/g T_{TSSP} values for both the alloys were comparable. Above this hydrogen concentration, the T_{TSSP} value for Zr–2.5Nb pressure tube material was observed to be higher than that for Zircaloy-2 pressure tube material. The maximum difference in the TSSP values for both the alloys (Fig. 7) was much lower compared to the difference between the TSSD values of the alloys (Fig. 6). In Fig. 7 the TSSP values obtained in the present investigation is also compared with TSSP values for these alloys reported in literature. It has been reported that the T_{TSSP} temperature is sensitive to the solution annealing temperature from which the sample is cooled, soaking time at the solution annealing temperature and rate of cooling from solution annealing temperature. For Zr–2.5Nb pressure tube alloy, it has been reported that for solution annealing temperature of 450 °C and above, T_{TSSP} temperature is independent of solution annealing temperature [47] and is designated as T_{TSSP1}. For a given hydrogen concentration and for solution annealing temperatures lower than 450 °C, T_{TSSP} is reported to increase with decrease in solution annealing temperature. For a solution annealing temperature just equal to T_{TSSD}, highest value of T_{TSSP} is obtained and is designated as T_{TSSP2} [47]. It has been suggested that the dependence of TSSP on solution annealing temperature is due to the formation of dislocation network in the matrix around hydrides [31,47]. If the solution annealing temperature is just above T_{TSSD} temperature, even though the hydride has dissolved the dislocation debris in the matrix around the preexisting hydrides remain and provides memory effect resulting in hydride precipitation during cooling at the pre-existing sites where hydrides were present before dissolution. A high solution annealing temperature anneals out the dislocation debris in the matrix. In such a case chemical free energy has to provide for plastic accommodation of hydride platelets leading to reduced T_{TSSP} temperature [66–68].

Thus a minimum solution annealing temperature is required to anneal the dislocation debris. Above this temperature any further increase in solution annealing temperature will not result in reduction in T_{TSSP} temperature unless the temperature is high enough to facilitate metastable β to stable β transformation [50–53]. The role of soaking time is to facilitate the kinetics of atomic movement to anneal out the dislocation debris. At lower solution annealing temper-

ature longer soaking time will be required while at higher solution annealing temperature shorter soaking time will be required to anneal out the dislocation debris left out in the matrix after hydride dissolution. Rate of cooling controls the size of the hydride precipitate. If a sample is cooled slowly after homogenization treatment, it will result in formation of larger hydride platelet and if during dilatometric measurement the sample is cooled at a faster rate compared to that after homogenization T_{TSSP} temperature changes. As can be seen from Fig. 7, the T_{TSSP} values obtained by McMinn et al. [61] for Zircaloy-2 and T_{TSSP2} values obtained by Pan et al. [47] for Zr–2.5Nb pressure tube alloys are comparable. In the present investigation, a solution annealing temperature of 430 °C and a soaking temperature of 30 min was used for both the alloys. The T_{TSSP} values obtained in the present investigation for the both the pressure tube material was comparable to the lowest T_{TSSP} temperature (T_{TSSP1}) value reported by Pan et al. [47]. This suggests that during the soaking at 430 °C for 30 min, the dislocation debris in the matrix might have been annealed out resulting in loss of memory effect for hydride precipitation and thereby lowest value of T_{TSSP} was obtained in the present investigation.

4.3. Enthalpy values

4.3.1. Zircaloy-2

The transition temperatures corresponding to the end of dissolution and start of precipitation of hydrides were obtained from the three methods described in Section 3.3 for Zircaloy-2 pressure tube material and were found to be comparable. The slope of the log of hydrogen concentration versus inverse of absolute transition temperature yielded the enthalpy of the dissolution or the precipitation process. The regression coefficient was greater than 90% for heating curve and greater than 95% for the cooling curve. The enthalpy of the hydride dissolution for Zircaloy-2 was in the range 30–34.5 kJ/mol while the enthalpy of hydride precipitation in this alloy was in the range 25.9–26.3 kJ/mol.

The TSSD and TSSP values as reported in literature are summarized in Table 4 [45,47,50,61,65]. The enthalpy of hydride dissolution and precipitation lie in the range 33.5–38.8 and 25.8–34.5 kJ/mol, respectively, for dilute zirconium alloy. Considering the fact that the transition temperature depend on the heating and cooling rate and were determined by different techniques, this kind of scatter in reported enthalpy values can be considered within the limits of experimental error. In the present investigation, the TSS values were obtained using dilatometry (listed in Table 3) and the enthalpies of dissolution and precipitation of hydrides in Zircaloy-2 pressure tube material were found comparable to the values reported in literature [45,47,50,61,65].

4.3.2. Zr–2.5Nb alloy

The transition temperatures obtained in the present investigation for Zr–2.5Nb pressure tube material from all the three methods described earlier were not as close as the transition temperature values for Zircaloy-2 pressure tube material. The enthalpy of hydride dissolution and precipitation in Zr–2.5Nb pressure tube alloy obtained in the present investigation were 35.4 and 17.5–22.8 kJ/mol, respectively with regression coefficients greater than 94% (Table 3). The enthalpy of dissolution of hydrides in Zr–2.5Nb pressure tube alloy obtained in the present investigation (35.4 kJ/mol) was comparable to the values reported for dilute Zr-alloy in literature (33.5–38.8 kJ/mol) [45,47]. However, the enthalpy of precipitation of hydrides in Zr–2.5Nb pressure tube alloy obtained in the present investigation (17.2–22.8 kJ/mol) was much lower than the values reported in literature (25.8–34.5 kJ/mol) [45,47]. Though most of the enthalpy values reported in literature for hydride precipitation in dilute zirconium alloys lie in the range of 25.8–34.5 kJ/mol, an enthalpy value of 19.9 kJ/mol has been reported for metastable Zr–10Nb alloy [52] which is close to the value obtained in the present investigation. However, the enthalpy values for hydride precipitation in Zr–10Nb alloy was determined in annealed condition having equiaxed microstructure and higher volume fraction of β Zr phase [52] as compared to the cold-worked and stress-relieved Zr–2.5Nb pressure tube alloy having heavily elongated α Zr grains with β Zr phase forming a thin but nearly continuous network along the grain-boundaries [60]. More work is under progress to resolve this and will be reported latter.

Table 4
Terminal solid solubility data for Eq. (1) reported in literature

S. no.	Material	Technique	TSS	A (μg/g)	ΔH_s (J/mol)	Ref.
1	Zr–2.5Nb PT	Dynamic elastic modulus (DEM)	TSSD	8.080×10^4	34520	[47]
2	Zr–2.5Nb PT	DEM	TSSP	2.473×10^4	25840	[47]
3	Zr–2.5Nb PT	DEM	TSSP	3.150×10^4	27990	[47]
4	Zr–2.5Nb	Dilatometry	TSSD	6.860×10^4	33570	[45]
5	Zircaloy-2	Dilatometry	TSSD	5.17×10^4	31500	[45]
6	Zircaloy-2	Differential scanning calorimetry (DSC)	TSSD	10.64×10^4	34629	[61]
7	Zircaloy-2	DSC	TSSP	13.87×10^4	34467	[61]
8	Zircaloy-2	Diffusion couple	TSSD	1.20×10^5	35900	[65]
9	Excel	DEM	TSSD	1.09×10^5	32600	[50]
10	Excel	DEM	TSSP	1.45×10^5	29900	[50]

4.3.3. TSS hysteresis

The amount of hydrogen in excess of solid solubility precipitates as solid hydride. Similar to any solid state phase transformation process the free energy of hydride precipitation has three components. These are chemical free energy, interfacial energy and strain energy. Chemical free energy term is required for the free energy associated with the transformation of matrix to hydride and is negative. Interfacial energy is required to create new interfaces and is positive. Hydrides occupy more volume than the metal from which it forms and hence is accompanied by positive misfit strains, which may result in generation of large internal stresses. Depending on the size of the hydride phase, the internal stresses could be large enough to induce local plastic deformation. Total strain energy stored in the material as a result of the accommodation of hydride precipitates in the matrix is called accommodation energy. For hydride precipitation under stress another term called interaction energy is considered. Interaction energy is the change in the strain energy of the matrix-precipitate system because of the applied, residual stress or the stresses due to the presence of other precipitates. Strain energy is the sum of the accommodation and interaction energy and is positive.

Based on the above line of arguments, Puls [33,62] developed a theoretical treatment of hydrogen TSS in these alloys, which defines an equilibrium TSS, C_0^T, for the case when no accommodation energy is required:

$$C_0^T = C_0 \exp\left(-\frac{\Delta H'_s}{RT}\right) \tag{3}$$

where C_0 is the pre-exponential constant and $\Delta H'_s$ is the enthalpy term. It was suggested that the accommodation energy is dependent on the size of the precipitate and its tendency to grow or dissolve leading to hysteresis behavior between the TSS obtained during heating and cooling [62]. During nucleation the accommodation energy is fully elastic whereas for a growing precipitate the accommodation energy is partly due to elastic and partly due to plastic deformation of the matrix and precipitate [66–68]. Usually interfacial free energy is neglected and in that case chemical free energy released due to phase transformation must provide for the strain energy required for inducing elastic and plastic deformation.The final TSS expression for the growth (cool down) and dissolution (heat up) of hydrides in terms of the stress-free solvus C_0^T defined in Eq. (3) is given in Eqs. (4) and (5), respectively [66–68].

$$C_0^{\text{growth}} = C_0^T \exp\left(\frac{\overline{W}_{\text{el,p}}^{\text{acc}} + \overline{W}_{\text{p}}^{\text{acc}}}{RT}\right) = C_0 \exp\left(-\frac{\Delta H'_s - \overline{W}_{\text{el,p}}^{\text{acc}} - \overline{W}_{\text{p}}^{\text{acc}}}{RT}\right) \tag{4}$$

and

$$C_0^{\text{diss}} = C_0^T \exp\left[\frac{\overline{W}_{\text{el,p}}^{\text{acc}} - \overline{W}_{\text{p}}^{\text{acc}}}{RT}\right] = C_0 \exp\left(-\frac{\Delta H'_s - \overline{W}_{\text{el,p}}^{\text{acc}} + \overline{W}_{\text{p}}^{\text{acc}}}{RT}\right) \tag{5}$$

The expression for strain energy associated with elastic, $\overline{W}_{\text{el,p}}^{\text{acc}}$, and plastic, $\overline{W}_{\text{p}}^{\text{acc}}$, accommodation are given in reference [33,62]. It may be noted that the strain energy stored in the material due to elastic deformation can be recovered but the strain energy spent in plastic deformation is partly locked in or around the defects and is partly dissipated in the form of sound, heat, etc. Thus, for a growing precipitate chemical free energy has to provide for strain energy associated with both elastic and plastic deformation whereas for dissolving precipitate strain energy associated with plastic deformation is not available and the part of the strain energy associated with elastic stress field around a plastically accommodated precipitate helps the dissolution process. And hence the expression for TSS obtained during dissolution (heat up cycle) should be modified as

$$C_0^{\text{diss}} = C_0^T \exp\left[-\frac{\overline{W}_{\text{el,p}}^{\text{acc}}}{RT}\right] = C_0 \exp\left(-\frac{\Delta H'_s + \overline{W}_{\text{el,p}}^{\text{acc}}}{RT}\right) \tag{6}$$

As is evident from Eqs. (4) and (6), the enthalpy of dissolution or precipitation is a function of enthalpy of the process corresponding to equilibrium solvus defined in Eq. (3) and components of strain energy of accommodation of hydrides in the matrix. It is clear from Eqs. (4) and (6) that the experimentally determined values of the enthalpy of dissolution and precipitation will differ by $2\overline{W}_{\text{el,p}}^{\text{acc}} + \overline{W}_{\text{p}}^{\text{acc}}$. Assuming hydrides as spherical precipitate with isotropic misfit strains, Puls [33] estimated a value of $\overline{W}_{\text{el,p}}^{\text{acc}}$, and $\overline{W}_{\text{p}}^{\text{acc}}$ as 0.5865 and 0.9555 kJ/mol of hydrogen at 300 K and thus suggesting a difference of 2.1285 kJ/mol between the enthalpies of hydride dissolution and precipitation in these alloys. The difference in the experimentally measured value of the enthalpy of dissolution and precipitation is about 5–8 kJ/mol for Zircaloy-2 pressure tube material and is of the order the theoretical prediction. Since accommodation energy is a function of yield strength of the material, the difference between the enthalpy of hydride dissolution and precipitation in Zr–2.5Nb pressure tube alloy is higher than that for Zircaloy-2 as the former possess higher yield strength compared to the latter.

5. Conclusions

TSS corresponding to end of dissolution and beginning of precipitation of hydrides in cold worked and stress-relieved Zircaloy-2 and Zr–2.5Nb pressure tube materials was deter-

mined from thermal strain versus temperature plots, average slope (of thermal strain versus T plots) versus temperature plots and differential strain versus temperature plots. The TSSD and TSSP values obtained from all the three plots were in good agreement for Zircaloy-2 pressure tube material. The TSSD and TSSP values for Zr–2.5Nb pressure tube material showed larger scatter compared to the scatter between the corresponding values for Zircaloy-2. The enthalpies of dissolution and precipitation of hydrides in Zircaloy-2 pressure tube material were 30.0–34.5 and 25.9–26.3 kJ/mol, respectively, which are comparable to the values reported in literature. The enthalpies of dissolution and precipitation of hydrides in Zr–2.5Nb pressure tube alloy were 34.5 and 17.2–22.8 kJ/mol. Though the enthalpy of dissolution of hydrides in Zr–2.5Nb pressure tube alloy is comparable to the values reported in literature, the enthalpy of hydride precipitation in this alloy obtained in the present investigation is much lower as compared to the enthalpy values reported in literature.

Acknowledgement

Authors express their sincere thanks to Head, Analytical Chemistry Division, BARC for hydrogen analysis by IGF technique.

References

[1] B.A. Cheadle, C.E. Coleman, H. Litcht, Nucl. Tech. 57 (1982) 413.
[2] W. Dietz, in: R.W. Cahn, P. Haasen, E.J. Kramer (Eds.), Nucl. Mater. 10B (1994) 53.
[3] C. Lemaignan, A.T. Motta, Nucl. Mater. 10B (1994) 1 (Chapter 7).
[4] D.L. Douglass, Atomic Energy Review, International Atomic Energy Agency, Vienna, 1971.
[5] E.F. Ibrahim, B.A. Cheadle, Can. Metall. Q. 24 (3) (1985) 273.
[6] R.G. Fleck, V. Perovic, E.T.C. Ho, Ontario Hydro Research Review No. 8 (1993) 1.
[7] C.E. Coleman, B.A. Cheadle, C.D. Cann, J.R. Theaker, in: E.R. Bradley, G.P. Sabol (Eds.), Zirconium in the Nuclear Industry, ASTM STP 1295, 1996, p. 884.
[8] J.R. Theaker, R. Choubey, G.D. Moan, S.A. Aldridge, L. Davis, R.A. Graham, C.E. Coleman, in: A.M. Garde, E.R. Bradley (Eds.), Zirconium in the Nuclear Industry, ASTM STP 1245, 1994, pp. 221–242.
[9] B. Cox, J. Nucl. Mater. 170 (1990) 1.
[10] J.H. Harding, J. Nucl. Mater. 202 (1993) 216.
[11] M.B. Elmoselhi, B.D. Warr, ASTM STP 1245 (1994) 62–77.
[12] K.N. Choo, Y.S. Kim, Su-I.I. Pyun, S.I. Pyun, J. Nucl. Mater. 226 (1–2) (1995) 9.
[13] C.E. Ells, J. Nucl. Mater. 28 (1968) 129.
[14] D.G. Westlake, J. Nucl. Mater. 26 (1968) 208.
[15] B. Nath, G.W. Lorimer, N. Ridley, J. Nucl. Mater. 58 (1975) 153.
[16] V. Perovic, G.C. Weatherly, C.J. Simpson, Acta Metall. 31 (1983) 1381.
[17] G.J.C. Carpenter, Acta Metall. 26 (8) (1978) 1225.
[18] G.C. Weatherly, Acta Metall. 29 (1981) 501.
[19] J.S. Bradbrook, G.W. Lorimer, N. Ridley, J. Nucl. Mater. 42 (1972) 142.
[20] D.G. Westlake, E.S. Fisher, Trans. Met. Soc. AIME (1962) 224.
[21] G.K. Dey, R.N. Singh, R. Tewari, D. Srivastava, S. Banerjee, J. Nucl. Mater. 224 (1995) 146–157.
[22] R. Dutton, Metall. Soc. CIM 16 (1978) (Annual volume).
[23] C.E. Ells, Metall. Soc. CIM 32 (1978) (Annual volume).
[24] J.B. Bai, C. Prioul, D. Francois, Metall. Mater. Trans. A 25A (1994) 1185.
[25] B.A. Cheadle, C.E. Coleman, M. Ipohorski, ASTM STP 824 (1984) 210–221.
[26] C.E. Ells, J. Nucl. Mater. 35 (1970) 306.
[27] M. Leger, A. Donner, Metall. Can. Q. 24 (3) (1985) 235.
[28] M.P. Puls, in: S. Saimoto, G.R. Purdy, G.V. Kidson (Eds.), Solute-defect Interactions, 1986, pp. 426–433.
[29] R.N. Singh, R. Kishore, S.S. Singh, T.K. Sinha, B.P. Kashyap, J. Nucl. Mater. 325 (2004) 26–33.
[30] R.N. Singh, Flow behavior and hydrogen embrittlement of Zr–2.5 wt.% Nb pressure tube alloy, Ph.D. Thesis, IIT Bombay (2002).
[31] D.O. Northwood, U. Kosasih, Int. Met. Rev. 28 (2) (1983) 92.
[32] S.Q. Shi, M.P. Puls, G.K. Shek, J. Nucl. Mater. 218 (2) (1995) 189.
[33] M.P. Puls, Metall. Trans. A 21A (1990) 2905.
[34] R.N. Singh, N. Kumar, R. Kishore, S. Roychoudhury, T.K. Sinha, B.P. Kashyap, J. Nucl. Mater. 304 (2002) 189–202.
[35] R.N. Singh, S. Roychowdhury, V.P. Sinha, T.K. Sinha, P.K. De, S. Banerjee, Mater. Sci. Eng. A 374 (2004) 342–350.
[36] R.N. Singh, S. Roychowdhury, R. Kishore, T.K. Sinha, P.K. De, S. Banerjee, BARC Report No. BARC/2003/I/03, 2003 pp. 1–88.
[37] A. Sawatzky, Can. Metall. Q. 24 (3) (1985) 227.
[38] H.D. Mair, M.D.C. Moles, M.P. Dolbey, IAEA Technical Committee Meeting, Mumbai, India, February 1994.
[39] Y.J. Kim, M.L. Vanderglas, Proceedings of the ASME-PVP Conference, New Orlearns, USA, June 1985, 1985, pp. 161–168.
[40] R.N. Singh, R. Kishore, T.K. Sinha, S. Banerjee, B.P. Kashyap, Mater. Sci. Eng. A 339 (2003) 17–28.
[41] R.N. Singh, R. Kishore, T.K. Sinha, B.P. Kashyap, J. Nucl. Mater. 301 (2002) 153–164.
[42] C.E. Ells, C.E. Coleman, B.A. Cheadle, S. Sagat, D.K. Rodgers, J. Alloys Compd. 231 (1995) 785–791.
[43] R.N. Singh, R. Kishore, S. Mukherjee, P.K. De, S. Bannerjee, Proceedings of the Second International Conference on Interactions of Hydrogen Isotope with Structural Materials, Sarov, Russia, April 12–17, 2004, 2004.
[44] W.H. Erickson, D. Hardie, J. Nucl. Mater. 18 (1964) 254.
[45] G.F. Slattery, J. Inst. Met. 95 (1967) 43.
[46] Y. Mishima, S. Ishino, S. Nakajima, J. Nucl. Mater. 27 (1968) 335–344.
[47] Z.L. Pan, I.G. Ritchie, M.P. Puls, J. Nucl. Mater. 228 (2) (1996) 227–237.
[48] S. Mishra, M.K. Asundi, Zr in Nuclear Applications ASTM STP 551, American Society for Testing and Materials, 1974, pp. 63–71.
[49] I.G. Ritchie, K.W. Sprungmann, Journal de physique, Colloque C9, supplement 12, Tome 44 December 1983, pp. 313–318.
[50] D. Khatamian, Z.L. Pan, M.P. Puls, C.D. Cann, J. Alloys Compd. 231 (1995) 488–493.
[51] D. Khatamian, V.C. Ling, J. Alloys Compd. 253–254 (1997) 162–166.
[52] D. Khatamian, J. Alloys Compd. 293–295 (1999) 893–899.
[53] D. Khatamian, J. Alloys Compd. 356–357 (2003) 22–26.
[54] R.W.L. Fong, S. Spooner, Scripta Metall. et Mater. 30 (5) (1994) 649.
[55] J.H. Root, R.W.L. Fong, J. Nucl. Mater. 232 (1996) 72–85.
[56] C.D. Cann, A. Atrens, J. Nucl. Mater. 88 (1980) 42–50.
[57] A. Sawatzky, B.J.S. Wilkins, J. Nucl. Mater. 22 (1967) 304.
[58] C.D. Williams, React. Technol. 13 (2) (1970) 147.
[59] A.M. Garde, E.R. Bradley (Eds.), Zirconium in the Nuclear Industry., ASTM STP 1245, 1994, p. 1. “Overview”.
[60] D. Srivastava, G.K. Dey, S. Banerjee, Metall. Trans. A 26A (1995) 2707.

[61] A. McMinn, E.C. Darby, J.S. Schofield, in: G.P. Sabol, G.D. Moan (Eds.), Proceedings of the 12th International Symposium on Zirconium in the Nuclear Industry, ASTM STP 1354, 2000, pp. 173–195.
[62] M.P. Puls, J. Nucl. Mater. 165 (1989) 128–141.
[63] C. Ganguly, in: P.K. De (Ed.), Proceedings of the Symposium on Zirconium, BARC, Mumbai, India, September 11–13, 2000, 2002, pp. 40–57.
[64] R.N. Singh, R. Kishore, S. Mukherjee, S. Roychowdhury, D. Srivastava, B. Gopalan, R. Kameswaran, S.S. Sheelvantra, T. K. Sinha, P.K. De, S. Banerjee, BARC Report No. BARC/2003/E/0341-49.
[65] J.J. Kearns, J. Nucl. Mater. 22 (1967) 292.
[66] M.P. Puls, Acta Metall. 8 (1984) 1259.
[67] M.P. Puls, Acta Metall. 29 (1981) 1961.
[68] B.W. Leitch, M.P. Puls, Metall. Trans. 23A (1992) 797.